Development of Reliable Gearless Motors for Electric Vehicles

Christopher H. T. Lee, *Member, IEEE*, K. T. Chau, *Fellow, IEEE*, and Libing Cao, *Student Member, IEEE*

Department of Electrical and Electronic Engineering, The University of Hong Kong, Hong Kong, China

In this paper, a new class of reliable gearless motors, dubbed as the magnetic steering (MS) motor, is proposed to realize the concept of the magnetic differential (MagD) system for direct-drive electric vehicles. While the electronic differential (ED) system can control two individual motors to provide the differential action in the absence of mechanical differential, it suffers from reliability concerns upon errors from the individual motors. The proposed MagD system instead utilizes the MS-field excitation to interlock the magnetic fields in two rotors of the MS motor. With the control of MS-field excitation, the two rotors can be differentiated to generate appropriate torque levels for two driving wheels. As a result, the MagD system can offer higher reliability than the ED system. The machine performances of the proposed MS motor are evaluated by finite element analysis and the operating performances of the proposed MagD system are testified by system level simulation.

***Index Terms*—Axial-flux, electronic differential, electric vehicle, gearless, magnetic differential, magnetic steering.**

I. Introduction

ELECTRIC vehicles (EVs) are the cleanest and greenest road transportation for smart cities [1], [2]. Conventionally, the two wheels of EVs are driven by a single traction motor with a mechanical differential (MD), to achieve both straight motion and curvilinear trajectory movement [3], [4]. However, this approach adopts the heavy and bulky differential gear, which is definitely not desirable for the EV system [5]. To get rid of this heavy, bulky and inefficient MD system, two or even more motors are separately installed beside the driving wheels so that each of them can be independently controlled to provide different speeds during concerning, and this is so-called the electronic or electric differential (ED) system [6], [7]. Based on the ED system, the differential gear can be eliminated and the overall weight and transmission loss of EVs can be significantly reduced. Yet, while the ED system can provide the differential action by controlling individual motors independently [8], fatal accidents might occur if there are any control or feedback errors from individual motors.

In order to simultaneously retain the merits of high safety and robustness of the MD system as well as attain the advantage of high compactness and accuracy of the ED system, the concept of magnetic steering machines was revealed [9]. Nevertheless, the corresponding principle of operation and how to make use of it to achieve the desired differential action are absent in literature.

In recent years, the development of magnetless doubly salient motors have been accelerated, with emphasis on the flux-switching DC (FSDC) topology [10], [11]. Because of the absent of rare-earth permanent magnets and the use of robust rotor structure, they are becoming attractive to serve as in-wheel gearless motors for EVs [12].

The purpose of this paper is to develop a new class of reliable gearless motors, which employs magnetic steering (MS) to realize the concept of the magnetic differential (MagD) system for direct-drive electric vehicles. By artfully incorporating the MS winding into the double-rotor (DR) FSDC motor, a new MS-DR-FSDC motor is proposed. The MS-field winding serves to produce an additional field excitation in such a way that it responds to the command of steering wheel and hence generates the MS flux to magnetically interlock the magnetic fields in the two rotors. During cornering, due to the presence of MS flux, the resultant flux at one rotor is strengthened while that at another rotor is weakened so that the two rotors can be driven with different torques to achieve the differential action. Since the MS flux provides the interlock mechanism with the magnetic mean, the proposed MagD system can definitely offer higher reliability than the ED system.

In Section II, the configuration and principle of the proposed MagD system will be described. In Section III, the machine structure and operation principle of the proposed MS-DR-FSDC motors will be discussed. Then, the machine performances of the proposed MS motors will be analyzed by using finite element method (FEM) in Section IV. Consequently, the operating performances of the proposed MagD system will be testified by system level simulation in Section V. Finally, a conclusion will be drawn in Section VI.

II. Proposed Magnetic Differential System

A. Vehicle Dynamic Modeling

Over the years, the dynamic modeling of engine vehicles has been well developed [13]. The corresponding model can readily be extended to EVs. In essence, the total tractive force F_{trat} of the EV is to provide an acceleration force F_a while overcoming the total resistive force F_{res}, which can be described as:

$$F_{tract} = F_a + F_{res} \tag{1}$$

$$\begin{cases} F_{res} = F_{roll} + F_{aero} + F_{slope} \\ F_{roll} = \mu Mg \\ F_{aero} = \dfrac{1}{2}\rho C_x S v^2 \\ F_{slope} = Mg\sin\alpha \end{cases} \tag{2}$$

where F_{roll} is the rolling resistance, F_{aero} is the aerodynamic drag force, F_{slope} is the slope resistance, μ is the rolling friction coefficient, M is the total mass of the EV, ρ is the air density, C_x is the aerodynamic drag coefficient, S is the frontal area of the EV, v is the linear speed of the EV and α is the slope of the road.

B. Curvilinear Movement

When the EV has to curve an angle, the exterior wheels have to run with a larger radius than the interior wheels do so that the ED system has to drive the wheels at different speeds. Precisely,

the exterior wheels have to spin at higher speeds than those of the interior ones. To describe the curve manoeuver, the simplified geometry model [7] is adopted as shown in Fig. 1. For instance, when the EV has to turn right, the linear speeds of two individual wheels v_L and v_R can be described as:

$$\begin{cases} v_L = \omega_{curve}(r + \frac{d}{2}) \\ v_R = \omega_{curve}(r - \frac{d}{2}) \end{cases} \quad (3)$$

where $\omega_{curve} = v / r$ is the angular speed of the curve, v is the linear speed of the EV, r is the radius of the curve, and d is the width of the EV. The radius of curve r can be further expressed as:

$$r = \frac{l}{\tan\delta} \quad (4)$$

where l is the length of the EV and δ is the turning angle.

When the EV is about to curve an angle, the steering signal is applied so that the exterior wheel has to increase its speed while the interior wheel instead has to decrease it. The difference between their angular speeds $\Delta\omega$ can be described as:

$$\Delta\omega = \frac{d\tan\delta}{l}\omega_{vehicle} \quad (5)$$

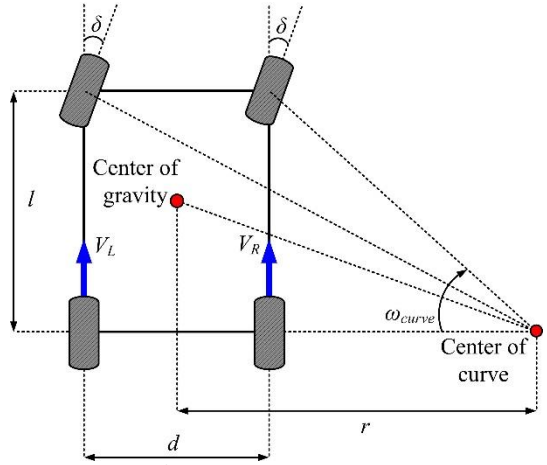

Fig. 1. Geometry model of an electric vehicle.

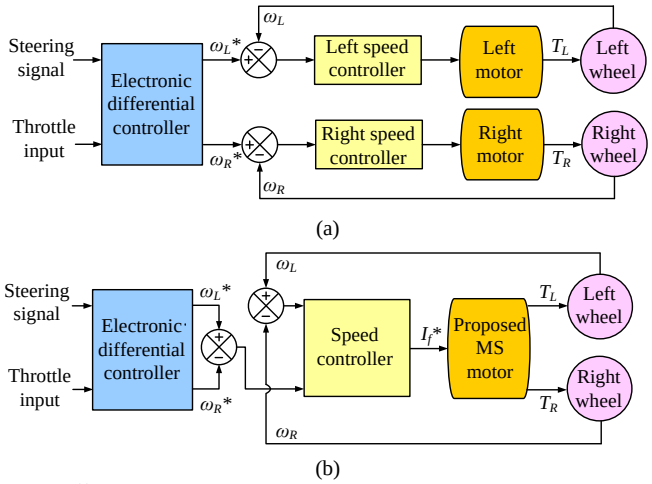

Fig. 2. Differential systems: (a) ED. (b) Proposed MagD.

where $\omega_{vehicle}$ is the angular speed of the EV. Consequently, the two speed references for the left and right wheels can be expressed as:

$$\begin{cases} \omega_L{}^* = \omega_L + \frac{\Delta\omega}{2} \\ \omega_R{}^* = \omega_R - \frac{\Delta\omega}{2} \end{cases} \quad (6)$$

For the ED system as shown in Fig. 2(a), the curvilinear trajectory movement can be accomplished based on independent control of two wheels. The two speed references ω_L* and ω_R* are fed into two speed controllers separately, hence generating two independent torques T_L and T_R to drive the left and right wheels, respectively. Even though the ED system can offer the desired differential action to curve an angle, it suffers from the bulky structure when using two motors for propulsion and the degraded reliability when using independent control of two wheels.

For the proposed MagD system as shown in Fig. 2(b), the curvilinear trajectory movement can instead be accomplished based on only one speed controller and one motor. To be specific, the speed difference reference between the two wheels $\Delta\omega$* is fed into the speed controller, and hence generates the MS-field current signal I_f* to control the MS-field excitation. Upon the regulation of the MS-field excitation, the proposed MS motor can differentiate the two output torques T_L and T_R based on the magnetic means, so as the wheel speeds. As compared with the ED counterpart, the proposed system can greatly improve the machine compactness and system reliability.

III. Proposed Magnetic Steering Motors

A. Machine Structures

To fully assess the proposed MS motors, two basic morphologies are evaluated – namely the radial-field (RF) and the axial-field (AF). Fig. 3 and Fig. 4 show the structures of the RF-MS-DR-FSDC motor and the AF-MS-DR-FSDC motor, respectively. Both of them employ the same pole arrangement that is derived from the profound three-phase 12/10-pole FSDC motor. The major distinction between the two motors comes from the flux flow directions: the flux path of the RF-MS-DR-FSDC motor flows along the radial direction, while that of the AF-MS-DR-FSDC motor flows along the axial direction. Upon the structure difference, the RF-MS-DR-FSDC motor is based on the sandwiched-stator concentric-rotor structure, while the AF-MS-DR-FSDC motor is based on the sandwiched-stator sided-rotor structure.

Similar to other FSDC motors, both of the proposed motors have the armature winding and DC field winding in the stator while their rotors have simple iron core with salient poles only. Differing from other FSDC motors, they incorporate the distinctive MS-field winding. This MS-field winding is purposely installed in such a way that it can offer flux strengthening and flux weakening towards the two armature windings in the stator. As a result, the two rotors can experience different torques, and hence the differential torque in the presence of MS-field excitation. Therefore, the differential action can be realized by only one control variable.

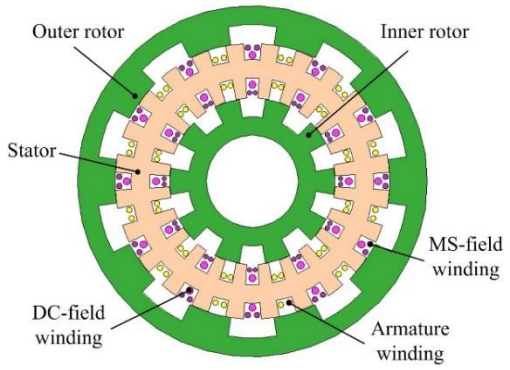

(a)

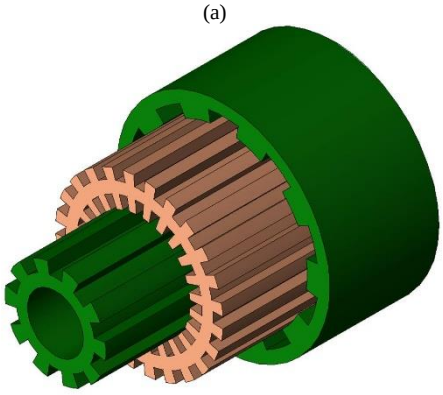

(b)

Fig. 3. Proposed RF-MS-DR-FSDC motor: (a) Configuration. (b) 3D view.

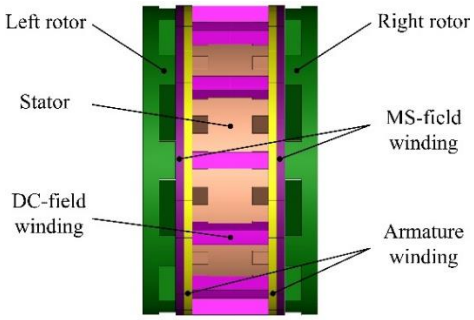

(a)

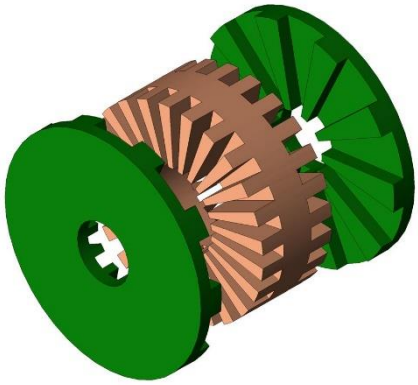

(b)

Fig. 4. Proposed AF-MS-DR-FSDC motor: (a) Configuration. (b) 3D view.

Since the proposed two motors are purposely developed for in-wheel motor drive applications, they are designed based on a typical wheel size of EVs. For instance, the wheel size of 195/65 R15 is adopted in which the axial length is of 195 mm and the rim diameter is of 15 in (381 mm). To have a fair comparison, the key motor dimensions, namely the outside diameters, inside diameters, stack lengths, airgap lengths and slot-fill factors of the two motors are set equal. Meanwhile, the pole arcs, pole heights and current densities are optimized to minimize magnetic saturation and so as the core losses.

B. Operation Principle

The proposed RF-MS-DR-FSDC and the AF-MS-DR-FSDC motors adopt the concentrated winding arrangements on the sandwiched-stator in such a way that the flux excited by the DC-field windings, dubbed as the DC flux, flow along the two rotors via the sandwiched-stator as depicted in Fig. 5. Meanwhile, the flux excited by the MS-field winding, dubbed as the MS flux, superimposes with the DC flux, hence creating the flux-strengthening effect at one side while the flux-weakening effect at another side. This is the key to make use of the MS flux to create the differential torque for the differential action during cornering. In principle, the DC-field windings can be wound with the concentrated winding arrangement, hence directly regulating the magnetic fields of two rotors individually. However, without the presence of MS-field winding, the two rotors will operate independently. Consequently, the magnetic interlock mechanism will be vanished, which can no longer provide the desired high reliability. Moreover, in inheriting the flux-switching characteristic, the flux-linkages of the these motors reverse their polarities in accordance with the rotor positions so that the iron core material can be fully utilized, hence achieving higher power and torque densities.

Since the inner and outer peripheral areas of the stator of the RF-MS-DR-FSDC motor are different, their electromagnetic interaction with the inner and outer rotors are different in nature. In contrast, the left and right peripheral areas of the stator of the AF-MS-DR-FSDC motor are identical so that their electromagnetic interactions with the left and right rotors are the same. As a result, the AF-MS-DR-FSDC motor inherently offers much better balancing properties between the two rotors than the RF-MS-DR-FSDC motor.

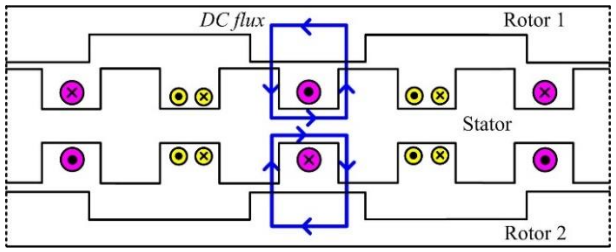

(a)

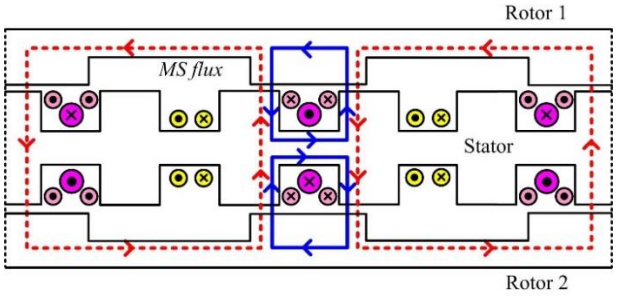

(b)

Fig. 5. Excitation fluxes in MS motors: (a) Without MS-field for straight motion. (b) With MS-field for cornering.

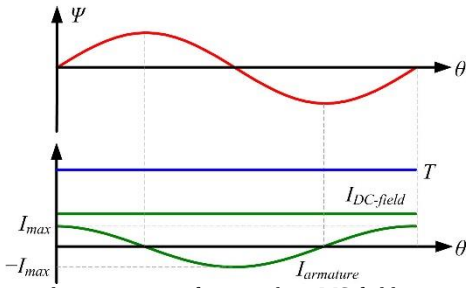

Fig. 6. Theoretical operating waveforms without MS-field.

C. Torque Production

The proposed MS motors can operate at the brushless AC (BLAC) mode or the brushless DC (BLDC) mode, depending the airgap flux waveform [3]. Since the BLAC operation can offer smoother torque than the BLDC operation, the proposed motors have been optimized to offer more sinusoidal flux-linkage Ψ. As illustrated in Fig. 6, when the DC-field winding current $I_{DC\text{-}field}$ is applied, the proposed motors will produce a theoretically constant electromagnetic torque T if the armature current $I_{armature}$ is applied in accordance with the flux-linkage. Meanwhile, there are the reluctance torque components as resulted from the feature of doubly salient poles. Since these reluctance torque components are small and exhibit an averaged zero value, the developed torques of the proposed MS motors are essentially contributed by the DC-field component.

When the EV has to turn a corner, the MS-field winding is excited accordingly. The resulting MS flux will superimpose with the DC flux, causing flux strengthening at one side and flux weakening at another side. The polarity of the MS-field winding current determines which side to be strengthened or weakened. Therefore, the torque production mechanism at each rotor is the same, while the torque difference between two rotors simply depends on the magnitude of the MS-winding current. Since the airgap flux densities at two rotors are regulated in a conjugated manner, a magnetically interlocking mechanism between the two rotors is created which can improve the reliability of the MagD system.

TABLE I. KEY DESIGN DATA OF PROPOSED MS MOTORS

Items	MS-RF-FSDC	MS-AF-FSDC
Radial outside diameter	381.0 mm	381.0 mm
Radial inside diameter	100.0 mm	100.0 mm
Airgap length	0.5 mm	0.5 mm
Axial stack length	195.0 mm	195.0 mm
No. of stator poles	12	12
No. of rotor poles	10	10
No. of phases	3	3
Slot-fill factor	60 %	60 %
No. of outer armature turns	52	N/A
No. of inner armature turns	38	N/A
No. of left armature turns	N/A	46
No. of right armature turns	N/A	46

IV. Machine Performance Analysis

A. Magnetic Field Distributions and Flux-Linkages

The key design data of the proposed MS motors are listed in Table I. To evaluate their performances, the electromagnetic field analysis is performed by using a well-developed FEM software package JMAG-Designer.

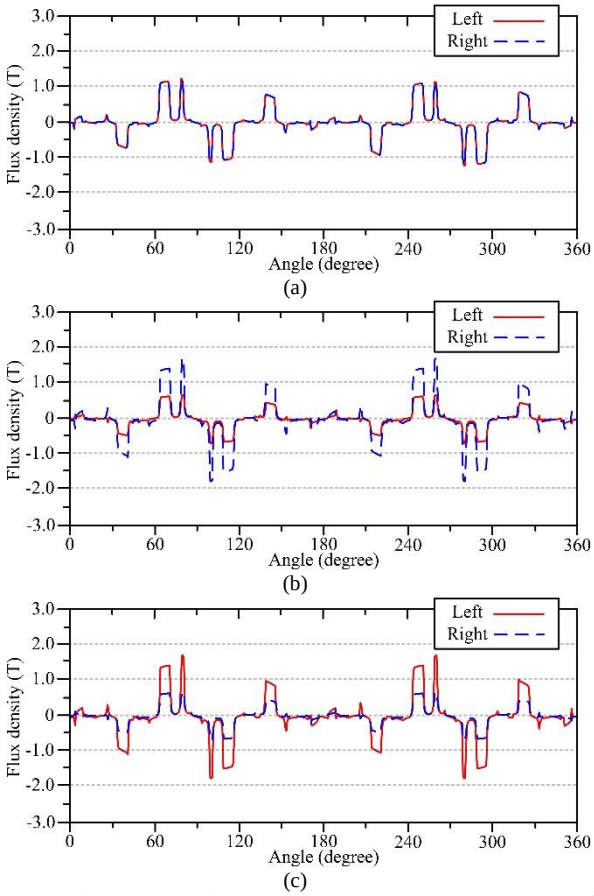

Fig. 7. Airgap flux densities of AF-MS-DR-FSDC motor: (a) Without MS-field. (b) With positive MS-field. (c) With negative MS-field.

The airgap flux densities of the AF-MS-DR-FSDC motor are shown in Fig. 7, where three situations are considered: namely without MS-field excitation, with positive MS-field and with negative MS-field excitation. Since the two motors produce similar flux patterns, the airgap flux densities of the RF-MS-DR-FSDC motor are omitted. It can be observed that when there is no MS-field excitation, the two sides of the AF-MS-DR-FSDC motor exhibit identical airgap flux densities. On the other hand, when the MS-field excitation is positively applied, the flux density in the right airgap is strengthened, while that of the left airgap is instead weakened. The situation is reversed when the MS-field excitation is negatively excited, namely the right side is weakened and the left side is strengthened. Similar findings also occur at the RF-MS-DR-FSDC motor, namely the inner and outer airgap fluxes resemble the left and right airgap fluxes. Therefore, the simulated results well agree with the theoretical expectation as depicted in Fig. 5, hence confirming the validity of the proposed MS-field regulation technique.

In addition, the flux-linkages of the proposed AF-MS-DR-FSDC motor under the DC-field excitation alone of 5 A/mm^2 are simulated as shown in Fig. 8. It can be seen that all the flux-linkages in each winding set are well balanced among three phases with bipolar characteristics. These results verify that the proposed motors can comply with that the profound FSDC motor does. Hence, the key design criteria such as the pole arrangement and the winding allocation are correct.

It should be noted the flux-linkage magnitudes between the two armature windings of the AF-MS-DR-FSDC motor are

identical. It is due to the fact the peripheral areas of the left and right sides of the stator are identical in nature. On the contrary, it can be anticipated that the flux-linkage magnitudes between the two armature windings of the RF-MS-DR-FSDC motor are different since the corresponding peripheral areas are different.

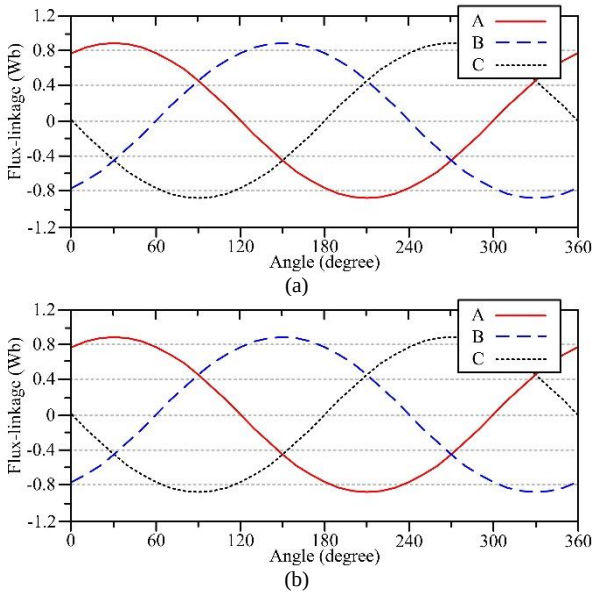

Fig. 8. Flux-linkage waveforms of AF-MS-DR-FSDC: (a) Left. (b) Right.

B. No-Load Electromotive Forces

The no-load electromotive forces (EMFs) of the two proposed motors under the DC-field excitation alone of 5 A/mm^2 at the base speed of 300 rpm can readily be deduced from the flux-linkage waveforms. As expected, the two proposed motors can both produce symmetrical no-load EMF patterns with no significant distortions. In addition, the no-load EMF waveforms essentially sinusoidal, which verify that they are favorable for BLAC mode of operation.

Inheriting from different flux-linkage magnitudes, the RF-MS-DR-FSDC motor produces different no-load EMF magnitudes between the inner and outer sides of the stator. It is expected because the peripheral area of the outer side is larger than that of the inner side. On the other hand, since the peripheral areas of the left and right sides are the same, the no-load EMF magnitudes of the AF-MS-DR-FSDC motor are identical.

C. Output and Cogging Torques

The output torque waveforms of the proposed motors under the DC-field excitations of 5 A/mm^2 are simulated as shown in Fig. 9. It can be observed that the rated average torques at the outer and inner rotors of the RF-MS-DR-FSDC motor are 110.2 Nm and 59.8 Nm, respectively. The corresponding torque ripples are 18.5% and 15.2%, respectively. On the other hand, the rated average torques at the left and right rotors of the AF-MS-DR-FSDC motor are 132.5 Nm and 132.2 Nm, respectively. The corresponding torque ripples are 21.5% and 21.4%, respectively. The results confirm that the two output torques of the AF-MS-DR-FSDC motor are almost identical, which is highly favorable for the proposed MagD system.

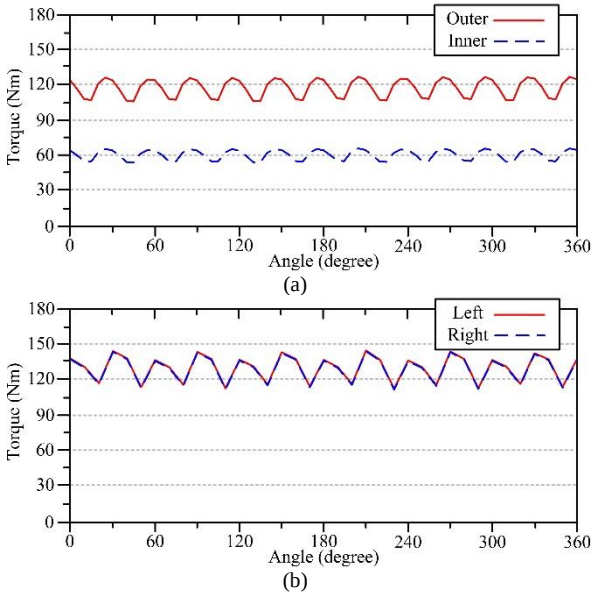

Fig. 9. Rated torque waveforms of proposed motors without MS-field: (a) RF-MS-DR-FSDC. (b) AF-MS-DR-FSDC.

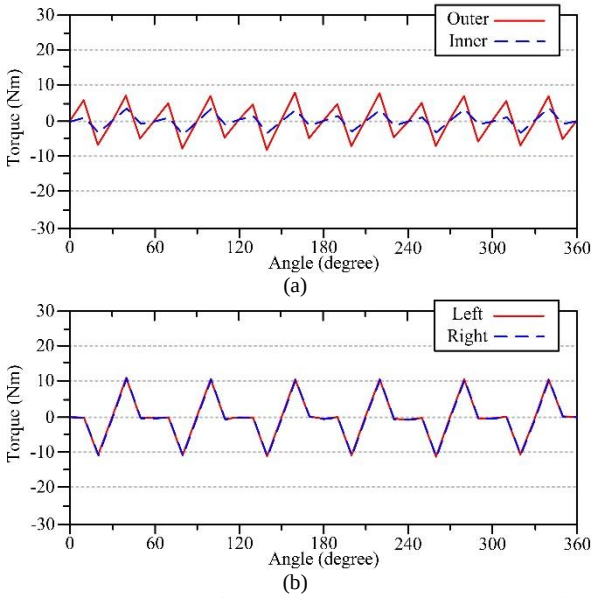

Fig. 10. Cogging torque waveforms of proposed motors without MS-field: (a) RF-MS-DR-FSDC. (b) AF-MS-DR-FSDC.

Furthermore, the cogging torque waveforms are simulated as shown in Fig. 10. It can be found that the peak cogging torque amplitudes of the RF-MS-DR-FSDC motor are 7.6 Nm and 3.8 Nm, respectively, while those of the AF-MS-DR-FSDC motor are 10.9 Nm and 10.7 Nm, respectively. These values are equivalent to 6.9% and 6.4% of its rated torque values for the RF-MS-DR-FSDC motor and 8.2% and 8.1% for the AF-MS-DR-FSDC motor. The cogging torques of the two proposed motors are relatively high because the designs have not yet adopted any means to reduce them at this stage. Actually, these cogging torques can be suppressed by applying the rotor skewing [14] or pole-arc optimization [15].

D. Differential Torques

Based on the above analysis, it is clear that the AF-MS-DR-FSDC motor is preferred to the RF-MS-DR-FSDC motor in

terms of torque balancing between two rotors. Thus, the AF-MS-DR-FSDC motor is further analyzed to evaluate its performance for the proposed MagD system.

Fig. 11 shows the output torque waveforms of the AF-MS-DR-FSDC motor when the MS-field windings are excited. It can be found that when the MD-field current is set at positive 5 A/mm^2, the average torques of the left and right rotors become 107.1 Nm and 142.7 Nm, respectively, hence turning a left corner. On the other hand, when the MS-field current is set at negative 5 A/mm^2, the average torques of the left and right rotors become 142.5 Nm and 106.8 Nm, respectively, hence turning a right corner. As a result, it confirms that the proposed MS-AF-FSDC motor can produce the same torque difference, namely the differential torque, between the two rotors for the desired curve trajectory movement.

Due to magnetic saturation, as compared with the torque values under no MS-field as shown in Fig. 9(b), the torque increments under the flux-strengthening effect of the MS-field are slightly less than the torque decrements under the flux-weakening effect of the MS-field. Nevertheless, this causes no harm to the proposed MagD system because the turning capability relies barely on the torque difference between the two rotors.

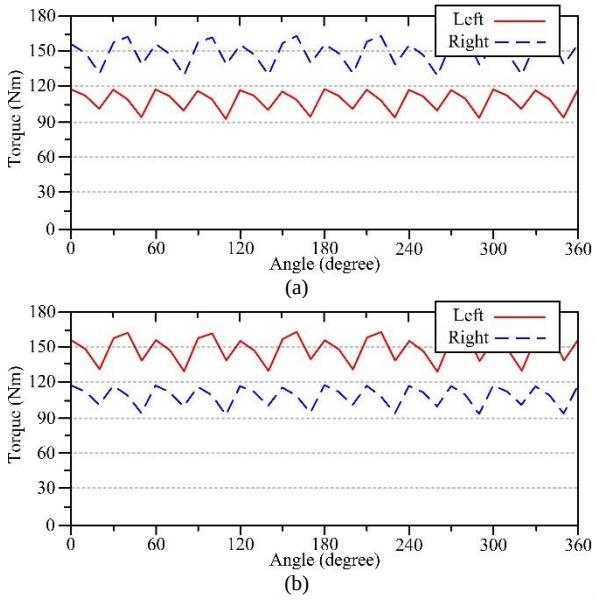

Fig. 11. Output torque waveforms of AF-MS-DR-FSDC motor with MS-field: (a) Positive excitation. (b) Negative excitation.

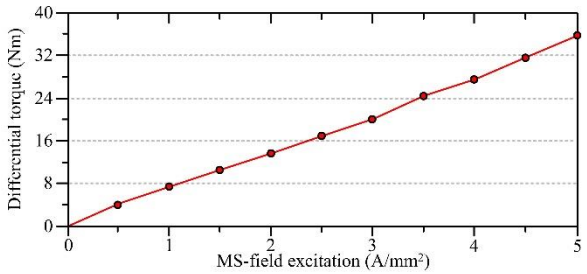

Fig. 12. Differential torque versus MS-field excitation characteristic of AF-MS-DR-FSDC motor.

Moreover, the differential torque versus MS-field excitation characteristic of the proposed AF-MS-DR-FSDC motor is plotted as shown in Fig. 12. It can be found that the relationship is almost linear which is very desirable for accurate steering control. In particular, under the 5 A/mm^2 MS-field excitation, the differential torque can reach 35.6 Nm which is very useful for effective cornering.

V. System Performance Analysis

A. Curvilinear Motion under Normal Operation

Based on (1)-(6), the curvilinear motion of an EV can be simulated by using MatLab/Simulink. The key parameters of the EV model are listed in Table II. When the motors are under normal operation, the vehicular performances of the ED system and the proposed MagD system with various turning angles are compared as shown in Fig. 13.

For the ED system, the curvilinear motion can be achieved by independently controlling the individual torques of two motors based on various turning angles. To be specific, at $\delta = 60°$, the EV is turning right with an angle of 60° degrees, while $\delta = -60°$ indicates that the EV is instead turning left with an angle of 60°. As illustrated, the speeds of the two wheels are differentiated accordingly while the speed of the EV is retained at the constant value of 30 km/h.

As compared with the ED system, the proposed MagD system can provide the same result upon the control of the MS-field current I_f. Specifically, I_f serves as the single parameter to differentiate the two torques for the two wheels. As depicted in Fig. 13(d), when $I_f < 0$, the driving torque at the left rotor is larger than that at the right rotor, hence turning right; when $I_f > 0$, the EV is turning left; when $I_f = 0$, it keeps straight motion. In general, various turning angles can be achieved upon different values of I_f.

B. Curvilinear Motion under Motor Fault

While the proposed MagD system can provide the same differential action as the ED system, it is imperative to testify its distinct merit on reliability. To make a fair comparison, both of the ED system and the proposed MagD system are subject to the same motor fault when the EV is turning right with an angle of 60° at the time instant of 8 s. For the ED system, this motor fault occurs at one of the two motors (for instance, the left motor); whereas for the proposed MagD system, the MS motor suffers from the same fault. This motor fault can be of various types, such as the short-circuit fault, open-circuit fault or inter-turn fault.

Fig. 14 compares the vehicular performances of the ED system and the proposed MagD system under the same motor fault. During fault, the motor cannot provide sufficient torque to meet the load torque so that the corresponding speed decreases accordingly.

TABLE II. KEY PARAMETERS OF EV MODEL

Parameters	Value
Total mass M	1200 kg
Rolling friction coefficient μ	0.015
Air density ρ	1.184 kg/m^3
Aerodynamic drag coefficient C_x	0.25
Frontal area S	1.9 m^2
Vehicle width d	1.5 m
Vehicle length l	2.5 m
Slope angle α	0 deg

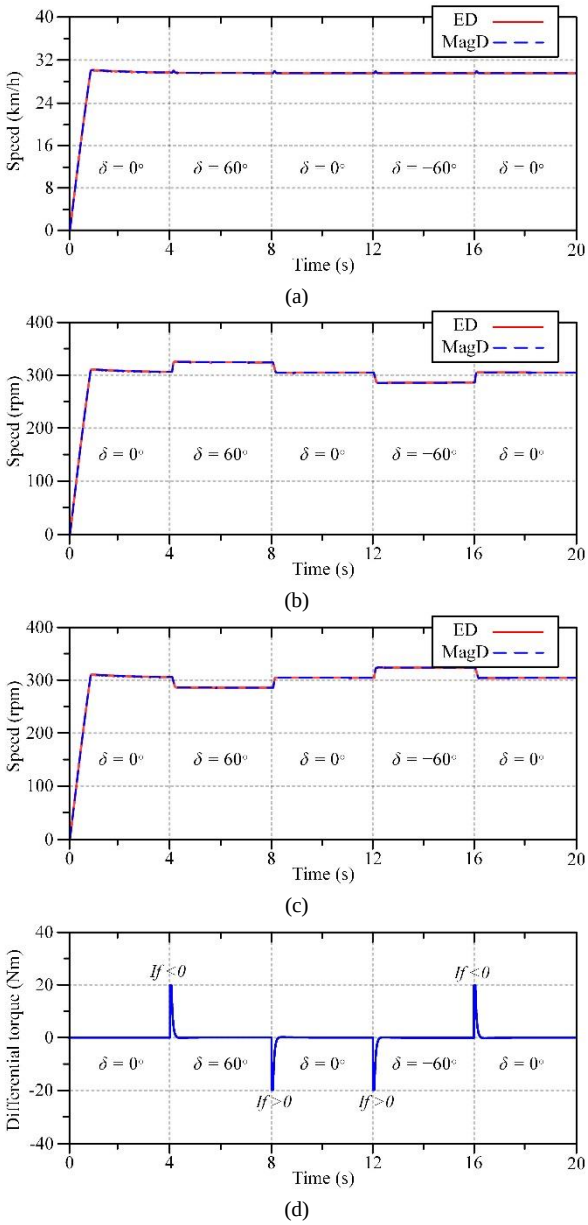

Fig. 13. Vehicular performances of ED system versus MagD system under normal operation: (a) Speed of EV. (b) Speed of left wheel. (c) Speed of right wheel. (d) Differential torque of MagD system.

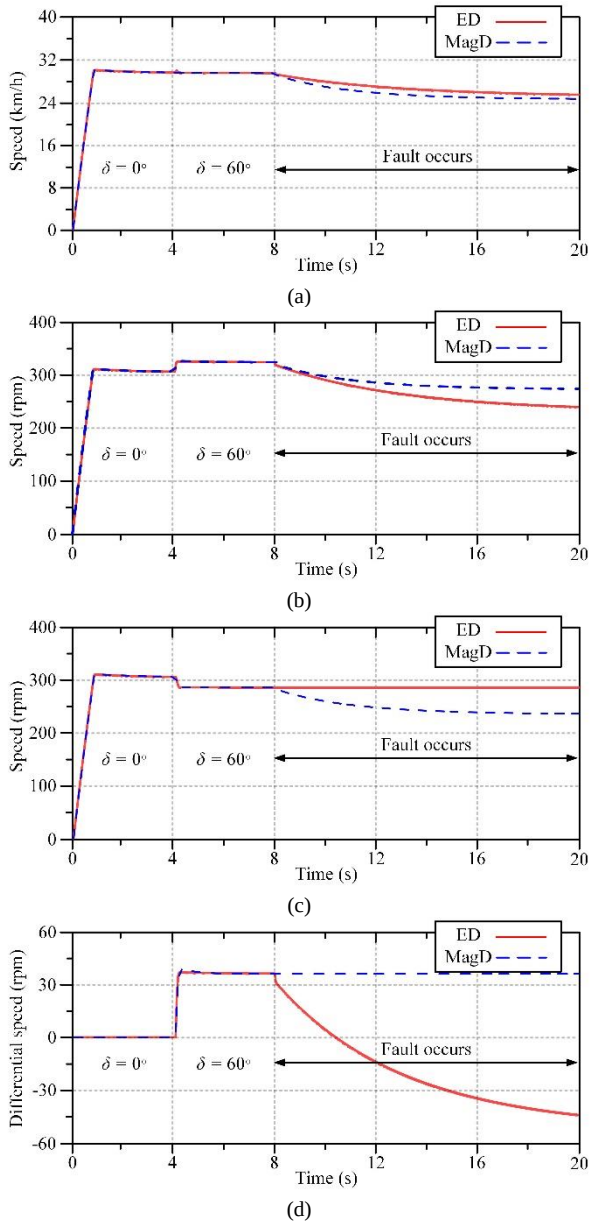

Fig. 14. Vehicular performances of ED system versus MagD system under motor fault: (a) Speed of EV. (b) Speed of left wheel. (c) Speed of right wheel. (d) Differential speed of two wheels.

For the ED system, the speed of left wheel decreases while the speed of right wheel keeps unchanged, hence the speed of EV starts to decrease from the time instant of 8 s. Thus, the differential speed between the left wheel and right wheel decreases from positive to negative as shown in Fig. 14(d). Consequently, the EV changes from turning right to turning left, which will cause a fatal accident.

In contrast, for the proposed MagD system, both the speed of left wheel and right wheel decrease concurrently since the left and right rotors are magnetically interlocked by the turning angle. As shown, the differential speed of the two wheels keeps at the same value. In other words, the EV is still turning right correctly although the vehicle speed has been reduced in the presence of motor fault. Therefore, it verifies that the proposed MagD system is much more reliable than the ED system.

VI. Conclusion

In this paper, a new class of reliable gearless motors, dubbed as the MS motor, has been proposed and applied to realize the MagD system for direct-drive EVs. The key is to utilize the magnetic interlocking technique of the MS motor to enable the MagD system offering the differential action for cornering. In particular, two MS motors, namely the RF-MS-DR-FSDC motor and the AF-MS-DR-FSDC motor, are quantitatively analyzed. With the control of MS-field excitation, the two rotors can be differentiated to generate appropriate torques for two driving wheels. Between the two MS motors, the AF-MS-DR-FSDC motor takes the advantages of higher torque density and better balancing, hence more favorable for the MagD system. System level simulation confirms that the proposed MagD system not only can provide similar curvilinear motion performance as the ED system under normal operation, but also

can maintain the differential action under motor fault, which might cause a fatal accident when using the ED system.

ACKNOWLEDGMENT

This work was supported by the Hong Kong Research Grants Council, Hong Kong Special Administrative Region, China, under Grant 17200614.

REFERENCES

[1] A. Emadi, Y. J. Lee, and K. Rajashekara, "Power electronics and motor drives in electric, hybrid electric, and plug-in hybrid electric vehicles," *IEEE Trans. Ind. Electron*., vol. 55, no. 6, pp. 2237–2245, Jun. 2008.

[2] W. Hua, G. Zhang, and M. Cheng, "Investigation and design of a high-power flux-switching permanent magnet machine for hybrid electric vehicles," *IEEE Tran. Magn*., vol. 51, no. 3, p. 8201805, Mar. 2015.

[3] K. T. Chau, *Electric Vehicle Machines and Drives–Design, Analysis and Application*. New York, NY, USA: Wiley, 2015.

[4] G. Tao, Z. Ma, L. Zhou, and L. Li, "A novel driving and control system for direct-wheel-driven electric vehicle," *IEEE Tran. Magn*., vol. 41, no. 1, pp. 497–500, Jan. 2005.

[5] J. Kim, C. Park, S. Hwang, Y. Hori, and H. Kim, "Control algorithm for an independent motor-drive vehicle," *IEEE Tran. Veh. Technol*., vol. 59, no. 7, pp. 3213–3222, Sep. 2010.

[6] N. Mutoh, T. Kazama, and K. Takita, "Driving characteristics of an electric vehicle system with independently driven front and rear wheels," *IEEE Trans. Ind. Electron*., vol. 53, no. 3, pp. 803–813, Jun. 2006.

[7] A. Draou, "Electronic differential speed control for two in-wheels motor drive vehicle," in *Proc. Fourth Int. Conf. Power Engineering, Energy and Electrical Drives*, May 2013, pp. 764–769.

[8] R. Wang, and J. Wang, "Fault-tolerant control with active fault diagnosis for four-wheel independently driven electric ground vehicles," *IEEE Tran. Veh. Technol*., vol. 60, no. 9, pp. 4276–4287, Oct. 2011.

[9] C. H. T. Lee, K. T. Chau, and C. Liu, "A new magnetic steering axial-field machine for electronic differential system in electric vehicle," in *Proc. International Magnetic Conference 2015*, May 2015, Paper No. AV–12.

[10] Y. Tang, J. J. H. Paulides, T. E. Motoasca, and E. A. Lomonova, "Flux-switching motor with dc excitation," *IEEE Tran. Magn*., vol. 48, no. 11, pp. 3583–3586, Nov. 2012.

[11] C. H. T. Lee, K. T. Chau, and C. Liu, "A high-torque magnetless axial-flux doubly-salient machine for in-wheel direct drive applications," *IEEE Tran. Magn*., vol. 50, no. 11, p. 8202405, Nov. 2014.

[12] X. Xue, W. Zhao, J. Zhu, G. Liu, X. Zhu, and M. Cheng, "Design of five-phase modular flux-switching permanent-magnet machines for high reliability applications," *IEEE Tran. Magn*., vol. 49, no. 7, pp. 3941–3944, Jul. 2013.

[13] R. N. Jazar, *Vehicle Dynamics: Theory and Applications*. New York, NY, USA: Springer, 2008.

[14] W. Fei, P. C. K. Luk, and J. Shen, "Torque analysis of permanent-magnet flux switching machines with rotor step skewing," *IEEE Trans. Magn.*, vol. 48, no. 10, pp. 2664–2673, Oct. 2012.

[15] C. H. T. Lee, K. T. Chau, and C. Liu, "Design and analysis of an electronic-geared magnetless machine for electric vehicles," *IEEE Trans. Ind. Electron*., vol. 63, no. 11, pp. 6705–6714, Nov. 2016.